Climate Risk Management 1 (2014) 5–24

Contents lists available at ScienceDirect

Climate Risk Management

journal homepage: www.elsevier.com/locate/crm

The probability of the impact of ENSO on precipitation and near-surface temperature

M.K. Davey [a,b,*], A. Brookshaw [a], S. Ineson [a]

[a] Met Office, Fitzroy Road, Exeter EX1 3PB, United Kingdom
[b] Dept. of Applied Mathematics and Theoretical Physics, University of Cambridge, Wilberforce Road, Cambridge CB3 0WA, United Kingdom

ARTICLE INFO

Article history:
Available online 27 December 2013

Keywords:
ENSO
Teleconnections
Regional climate
Seasonal temperature
Seasonal precipitation

ABSTRACT

The widespread influence of El Niño Southern Oscillation (ENSO) events on regional climate is well known, and such events can have considerable socio-economic impact. Thus an aspect of practical importance is the chance of the occurrence of various climate categories given that ENSO conditions are predicted or underway. Using observational and re-analysis datasets for precipitation and near-surface temperature this aspect is analysed systematically in terms of three near-equiprobable categories (below normal, near normal, above normal) to quantify the probability of their occurrence when central-east equatorial Pacific sea surface temperatures are abnormal, as during El Niño and La Niña events, with emphasis on land areas and on seasonal (three-month average) values. By using recently available gridded datasets, this analysis complements and updates previous analyses of ENSO impact. Spatial maps of the rate of occurrence of various categories conditional on ENSO state are obtained by point-by-point analysis of the global datasets. Consistent with previous analyses, several regions with rates well above those expected by chance are identified, in both tropical and extratropical sectors. Regional averages are used to examine a selection of these in more detail, in particular to describe the strong seasonal dependencies of ENSO influences. These depend on the interplay between the seasonality of ENSO, of teleconnection pathways and of local climate: indeed in several locations opposite effects arise at different times of year.

The methodology is based on contingency tables calculated from historical records, and effectively quantifies the probability that, for example, above-normal rainfall will occur in a given season and location conditional on the state of equatorial Pacific sea surface temperature. The rates of occurrence provide more directly relevant information for risk assessment and management than do statistics such as correlations or composites. Each ENSO event is different and occurs in conjunction with other climatic factors, so while the historical rates provide general guidance they should not be regarded as a prediction of impacts for a particular imminent or ongoing ENSO event.

Introduction

On interannual timescales the El Niño Southern Oscillation (ENSO) phenomenon is the dominant mode of climate variability. Months-long episodes of above-normal (El Niño: denoted EN hereafter) and below-normal (La Niña: LN hereafter) sea

* Corresponding author at: Dept. of Applied Mathematics and Theoretical Physics, University of Cambridge, Wilberforce Road, Cambridge CB3 0WA, United Kingdom. Tel.: +44 (0)1223 764060.
E-mail addresses: mike.davey@metoffice.gov.uk, mkd3@cam.ac.uk (M.K. Davey).

2212-0963
http://dx.doi.org/10.1016/j.crm.2013.12.002

surface temperature (SST) in the equatorial Pacific are accompanied – and reinforced – by changes in atmospheric circulation. Through atmospheric dynamical processes, such changes extend well beyond the tropical Pacific, and influence, for example, the patterns of seasonal winds, rainfall and temperature worldwide. These 'teleconnection' effects in turn have substantial socio-economic impacts (see e.g. Glantz, 1996; Couper-Johnston, 2000), so estimating the likely climatic consequences of ENSO events is an important aspect of managing the associated risks.

The important impacts of ENSO have motivated the enhancement of ocean and atmosphere observing systems, particularly for the tropical Pacific Ocean, and of efforts to understand the physical processes, in order to improve capacity to monitor and predict events (see e.g. Trenberth et al., 1998). Through the large-scale coupled ocean–atmosphere interactions involved in the development and evolution of ENSO events, the occurrence of such events is highly predictable several months in advance, so actions can be taken to limit adverse effects or take advantage of favourable conditions – for example in the agricultural sector through the selection of appropriate crops – taking into account uncertainties in the impacts. Prediction of ENSO and its impacts is a major component of seasonal forecasting activity – see e.g. Troccoli et al. (2008).

The climatic effects of ENSO, which vary substantially with region and season, can be quantified by analysing historical records. Composites of conditions observed during EN and LN events provide useful estimates of what to expect. However the 'usual' effects do not always occur: though often dominant, ENSO events are just one aspect of the climate system; moreover, individual events differ in details such as location, timing and magnitude.

The Met Office is one of a number of centres that produce and distribute long-range forecast (LRF) information – usually in the form of seasonal averages at lead times up to several months ahead – and as such frequently receives queries regarding the 'typical' effects of ENSO and their likely occurrence. To help address such questions an analysis of historical data has been made, and in this article we aim to summarise the methodology and results of that investigation. Note that this is distinct from forecasting the effects of an imminent or current ENSO event: for that purpose, the data from dynamical LRF systems provide information that includes the effects of many components of the climate system and as such is more relevant and more accurate than historical statistics.

To reduce the effects of month-to-month fluctuations, seasonal (3-month) averages are commonly used in investigations of ENSO effects. For brevity, December–January–February will be denoted DJF or season 1, and similarly for other seasons. The season number will correspond to the calendar month of the middle of the three months in the season. A list of acronyms and abbreviations is provided in Table 7.

Previous estimates of ENSO effects

There is a very extensive literature on regional ENSO effects. Here we summarise some of the global analyses for near-surface temperature (denoted T for brevity) and precipitation (denoted PR).

The best-known analyses are those for PR by Ropelewski and Halpert (1987, 1989, 1996) and for T by Halpert and Ropelewski (1992). In particular, their schematic summary global maps of ENSO effects on precipitation and near-surface temperature have been widely used and adapted: see e.g. Fig. 21 in Ropelewski and Halpert (1987) for EN and PR, Fig. 18 in Ropelewski and Halpert (1989) for LN and PR; Fig 13 in Halpert and Ropelewski (1992) for EN and LN and T.

Ropelewski and Halpert (1987, 1989, 1996) analysed station data of precipitation in the period 1875–1992, using composites for individual stations and regional aggregates. EN and LN events were selected using the Southern Oscillation Index (SOI), which is an atmospheric measure of ENSO activity: an EN (LN) event was defined by SOI in the lower (upper) 25% for at least 5 months. The first harmonic in a 24-month period (July a year before to June a year after) was used to characterise the typical evolution through an event. (For most locations the relation between precipitation anomalies and ENSO evolution was sufficiently simple for one harmonic to be effective in characterising relationships.) Nineteen regions with coherent substantial impact were selected subjectively for more detailed analysis. The tables of regional statistics include the number of individual 'wet' and 'dry' occurrences for EN or LN categories: see e.g. Table 2 in Ropelewski and Halpert (1987, 1989). (The number of cases varies from region to region, as observational data coverage varies greatly in space and time.) The probability of reaching or exceeding these categorised numbers by chance could be calculated from the hypergeometric distribution (see below), thus providing an estimate of confidence that the numbers did not arise by chance. (Typically a chance of 5–10% is regarded as significant for such analyses.) Only in the central Pacific were 100% rates (all wet or all dry) found; elsewhere the highest rates occurred in eastern South America.

Halpert and Ropelewski (1992) likewise analysed station data for temperature in the period 1886–1988, using composites of EN and LN events, identifying about 12 regional timeseries for more detailed analysis. Tables 3 and 4 in Halpert and Ropelewski (1992) include regional 'cold' and 'warm' occurrence rates. As with PR, the sign and seasonality of ENSO effects varies considerably with location: for example, in their 'Northern Australia' region high 'cold' and 'warm' rates were found for both EN and LN states, depending on the season.

Kiladis and Diaz (1989) similarly calculate composite T and PR using station data covering 1877–1982, with ENSO events defined using both SOI and east equatorial Pacific SST. They provide and describe composite differences (EN minus LN) for 3-month seasons leading up to and following an ENSO episode. A 'percentage of consistent signals' measure is defined as the percentage of events with anomalies consistent with the sign of the composite: thus information from EN and LN events is combined in their analysis. With this categorisation, confidence levels were estimated from the hypergeometric distribution. Statistics including percentage of consistent signals for representative stations (17 for T, 22 for PR) were tabulated. A composite for SST was also provided, illustrating the widespread nature of SST anomalies associated with ENSO.

Mason and Goddard (2001) made use of a gridded dataset of monthly PR (an analysis of station data) for the period 1951/52 to 1995/96. Selection of EN and LN events was based on the Niño3.4 (N34 hereafter) index. This index is SST averaged over a region of the east-central equatorial Pacific (5S–5N, 170W–120W), which is one of several such oceanic indices commonly used for ENSO. Seasonal data were categorised with three equally populated groups (above-, near-, below-normal PR) and the 8 strongest EN and LN events in this period. (Similar results were reported when selecting 5 or 11 EN and LN events.) Confidence levels regarding numbers in the categories were based on the hypergeometric distribution, for which the appendices in Mason and Goddard (2001) contain useful discussions. Maps of numbers for LN and EN with above- and below-normal PR were provided for DJF, MAM, JJA, SON seasons, with accompanying descriptions of the principal features. This approach was the basis of a later report (Someshwar, 2009) on the impact of EN, which contains regional maps of increases in odds of above- and below-normal PR in EN conditions for JAS, OND and JFM seasons, along with various socioeconomic indicators.

Atmospheric reanalyses, in which quality-controlled atmospheric observations are combined and processed using a comprehensive dynamical atmospheric model, provide alternative sources of gridded data for recent decades, with the advantage of complete spatial and temporal coverage. Seasonal reanalysis T data agree well with station-based estimates, but PR estimates are less reliable. (Note that while T observations are assimilated in reanalyses, observed PR data are not.) Yang and DelSole (2012) made use of NCEP (National Centers for Environmental Prediction) reanalysis T and a separate gridded set of PR station data in the period 1948–2010, together with the N34 index, to calculate spatial regression patterns over land for the DJF and JAS seasons. The results provide another view of the teleconnection patterns associated with ENSO, with features broadly similar to those found in other analyses: see e.g. the spatial maps in their Figs. 4–7. Such patterns also provide a useful means of assessing the performance of climate models with regard to their ability to represent ENSO effects, and the patterns found in several such models are provided for comparison in Yang and DelSole (2012).

A common feature of these ENSO effects is the symmetry of EN and LN impacts: e.g. in locations where EN is associated with higher than usual values, LN is very often – but not always – associated with lower than usual values. Thus some analyses combine EN and LN effects by investigating differences (this has the advantage of increasing sample size and thus significance), while some treat them separately.

Analyses have also been made of ENSO-related sub-seasonal behaviour. Using station T and PR data and daily and 5-daily statistics, Kenyon and Hegerl (2008, 2010) investigated the influence of three climate modes, including ENSO in the period 1896–2004, with emphasis on the occurrence of extremes (90th and 95th percentiles). Spatial maps of the influence of EN and LN events are provided: see e.g. their Figs. 2–4. Patterns of such influences are generally similar to ENSO effects on seasonally-averaged quantities: to give one example, in southeastern Africa where EN is associated seasonally with above-average summer T, there is a tendency for more frequent occurrence of 'extreme' warmer nights and days in EN conditions.

Analyses of historical data also provide predictive information, and there are many examples of ENSO indices being used as statistical predictors for regional climate. One example with a global scope is that of Stone et al. (1996), in which 5 phases (effectively categories) of SOI were used to estimate the probability of exceeding median rainfall in subsequent seasons.

Further information about ENSO and its impacts can be found on the websites provided by several climate centres: see for example http://www.knmi.nl/research/global_climate/enso/effects/, http://iri.columbia.edu/climate/ENSO/globalimpact/index.html, http://www.esrl.noaa.gov/psd/enso/enso.climate.html, http://www.metoffice.gov.uk/research/climate/seasonal-to-decadal/.

As climate variations occur on decadal and multidecadal scales, it is possible that the effects of ENSO also vary on those timescales, through changes in ENSO types and through changes in atmospheric circulation that influence teleconnection pathways. Van Oldenborgh and Burgers (2005) and Sterl et al. (2007) have demonstrated that observed changes may arise by chance, making it difficult to establish physical causes.

Datasets

We have used several gridded analyses that provide monthly-mean values with near-global coverage. For precipitation, data were used for 1979–2012 from the Global Precipitation Climatology Project (GPCP, version 2.2, Adler et al., 2003), and for 1979–2010 from the NCEP CPC (Climate Prediction Center) Merged Analysis of Precipitation (CMAP, Xie and Arkin, 1997). These make use of ground observations and data from remote (e.g. satellite-borne) instruments: for both, the analysed data have 2.5 by 2.5 degrees latitude–longitude resolution.

For near-surface temperature, the NCEP reanalysis (Kalnay et al., 1996) dataset provides near-surface T with 2.5 by 2.5 degrees latitude–longitude resolution for 1948 onwards. The CRUTEM anomaly dataset based on station data (Jones et al., 2012; Morice et al., 2012) contains values aggregated on a 5 by 5 latitude–longitude grid for 1850 to near real time. This dataset is quite sparse in some regions, but has the advantage of longer temporal coverage. Version 4.1.1.0 was used for the calculations in this paper. We also made use of T at 2 m height from the ERA-interim reanalysis, with higher spatial (0.75 by 0.75 degrees) resolution but a shorter time domain (1979–2012, Dee et al., 2011), but for brevity the results are not reported here.

As an index for ENSO, we use Niño3.4 averages calculated from the HadISST SST dataset, which has 1 by 1 degrees latitude–longitude resolution for 1870 to near real time (Rayner et al., 2003).

For each dataset seasonal values were calculated by applying a simple three-month running mean.

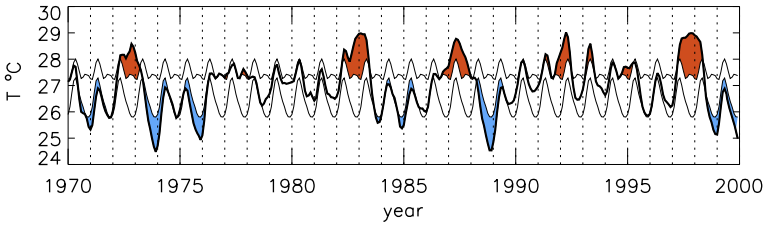

Fig. 1. A sample of the Niño3.4 timeseries, thresholded at the 25% and 75% levels using 1951–2010 data, showing the 1970–2000 portion. The thick line is the observed value, and thin lines indicate the seasonal cycle of the threshold values. Observed values above the upper threshold are classified as EN, indicated by red infill between observed and upper threshold, and values below the lower threshold are classified as LN, with blue infill. (For interpretation of the references to colour in this figure legend, the reader is referred to the web version of this article.)

Methodology

The essence of the method is the calculation of contingency tables based on three 'ENSO' categories and three target categories, where the target may be gridpoint or regionally-averaged T or PR, using seasonal values. This approach has the advantage that no assumptions about distributions or climate averaging periods are necessary, and moreover the method is easy to explain and does not require specialist climatic or statistical expertise to understand.

Definitions of ENSO events vary, but for the oceanic component they usually involve indices based on regionally-averaged SST for one or more standard regions in the equatorial Pacific. We opted to use N34 as it is widely used and covers various 'flavours' of ENSO events. (No attempt to subdivide ENSO events into e.g. East Pacific or Central Pacific types is made here. That could be the basis for further investigation, but the limited number of sub-type events increases the uncertainty of results.)

The 25% and 75% levels were chosen as the thresholds, based on actual (rather than anomaly) seasonal values of N34. For n years, categorisation is such that the EN and LN categories have the same number of entries, denoted nEN and nLN: thus nEN = nLN = $n/4$ rounded up to the nearest integer. For example, taking all JFM values of N34 in say a 32-year sample, the top 8 values are classified as EN, the bottom 8 are classified as LN, and the intermediate 16 are neutral. Note: a very few isolated outer category seasons that are not part of a recognised EN or LN event thus arise, which are shorter-lived SST 'extremes' rather than ENSO events. Their inclusion has little effect: a test with a 20% threshold gave similar results with regard to impacts (cf Mason and Goddard, 2001).

The upper and lower thresholds, and their difference, vary substantially seasonally: the difference is largest near the end of the calendar year. There is often a rapid transition from EN to LN categorisation, such as in 1973 in the sample in Fig. 1. Another feature demonstrated in Fig. 1 is that although the 1991/92 EN event was not exceptional in terms of SST anomalies (departures from seasonal climatology), actual SST in early 1992 was nearly as high as the peak in the major 1982/1983 and 1997/98 EN events. There is similar behaviour in mid-1987.

For PR and T the data are separated into three equally or nearly-equally populated categories for each season. In a sample of n years, the high and low (denoted HI and LO for brevity) categories with nHI and nLO members respectively are selected such that nHI = nLO = $n/3$ rounded up to the nearest integer. There is a trade-off between the 'extremity' and the sample size of the HI and LO categories: the choice here (commonly used in such analyses) is simple in form, and effective in providing a broad indication of significant ENSO effects. Note that for some regions and seasons the threshold of about one third may be a small departure from the climate mean, and although events in the outer categories may have a strong ENSO association they may not have significant practical consequences. Certainly for particular locations and applications a more tailored analysis would be required for risk management purposes.

(As a rough guide, for a Gaussian distribution the upper 25% corresponds to values more than 0.67 standard deviations above the mean, the upper 33% corresponds to more than 0.44, and the upper 20% corresponds to more than 0.84.)

The category boundaries depend somewhat on the years sampled. We opted to categorise based only on the years to be analysed: e.g. in processing 1979–2010 PR data we categorised ENSO using 1979–2010 N34 data, even though the N34 dataset is much longer. The effect is small: for N34 JFM for example, the boundaries are 26.22 and 27.26 °C for 1911–2010, 26.19 and 27.23 for 1951–2010, 26.19 and 27.26 for 1979–2010.

No detrending was applied for the results shown in this article. The effects of linear detrending of both N34 and of T and PR timeseries were tested, and found to be generally small.

For a given season and a sample of n categorised years of N34 and the impact variable (T or PR), a 3 by 3 contingency table can be constructed. The number of events in the EN and HI category is denoted n(HI and EN) etc., and the proportion of EN events with HI values is n(HI and EN)/nEN, etc. The latter ratio is the rate of occurrence of HI events given EN conditions, which can be regarded as an *estimate* of the conditional probability that HI will occur given EN oceanic conditions.

A typical regional example is provided in Fig. 2, which shows a scatterplot of N34 and standardised T values for DJF in the MexicoUSA region, together with the category boundaries, and the accompanying contingency table (see Table 1 for regional definitions).

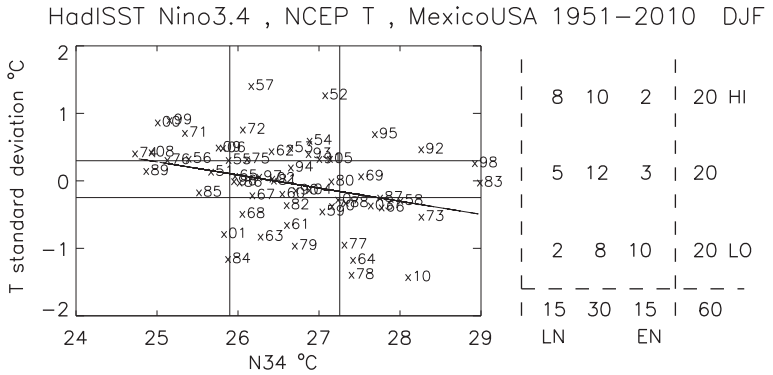

Fig. 2. The scatterplot shows NCEP T, averaged over the region 26N–35N, 103W–85W, versus Niño3.4 SST, both for the DJF season, for 1951–2010. The T data are standardised anomalies. The sloping line is a best-fit linear regression. The horizontal and vertical lines on the scatterplot indicate the boundaries between categories. The points are labelled by the year of the middle month of the season: e.g. 73 is the season comprising Dec1972, Jan1973 and Feb1973. The corresponding contingency table is on the right, including sums of the rows and columns.

Table 1
Regions defined for temperature averages which are calculated using land points in the areas indicated. Names are just indicative. For CRUTEM data, only locations with temporal coverage greater than the percentage indicated are used in the calculation. For some regions the years 1951–2010 were selected instead of 1911–2010 to achieve over 95% coverage at most points within the region, and for 'insufficient' regions this criterion was not met.

Name	Location	CRUTEM data selection
NSAmerica	15S–10N, 80W–50W	1951–2010 95%
CSAmerica	30S–15S, 72W–45W	1911–2010 95%
SSAmerica	45S–30S, 72W–54W	1911–2010 100%
MexicoUSA	26N–35N, 103W–85W	1911–2010 100%
NWNAmerica	45N–65N, 145W–120W	1911–2010 100%
NENAmerica	45N–55N, 90W–65W	1911–2010 100%
India	16N–26N, 72E–89E	1911–2010 100%
SEAsia	5N–20N, 95E–110E	1951–2010 95%
Japan	30N–42N, 132E–145E	1911–2010 100%
Indonesia	10S–0, 100E–125E	Insufficient
NEAustralia	25S–10S, 140E–150E	1911–2010 100%
SEAustralia	40S–25S, 143E–155E	1911–2010 100%
SWAustralia	35S–30S, 115E–125E	1911–2010 99%
NewZealand	50S–35S, 165E–180E	1911–2010 100%
NSAfrica	15S–0, 10E–40E	Insufficient
SSAfrica	30S–20S, 18E–35E	1911–2010 95%
WAfrica	6N–16N, 14W–2W	1951–2010 95%
NWAfrica	25N–35N, 15W–2W	Insufficient
SEurope	40N–50N, 0E–20E	1911–2010 99%
NWEurope	50N–70N, 5E–45E	1911–2010 100%

Abbreviations used for the regional names are, for example, NWNAmerica for north-west North America; CSAmerica for central South America.

In this example, of the 15 'EN' cases T was in the LO category on 10 occasions and in the HI category twice, and of the 15 'LN' cases T was in the HI category 8 times and in the LO category twice. Thus the rate of occurrence for LO T given EN is n(LO and EN)/nEN = 10/15. The clustering of values near, for example, the HI T boundary in LN conditions in Fig. 2 is an indication that counts can easily vary by one or two and accordingly rates are correspondingly imprecise. Seasonal cycles of rates as described in Section 'Near surface temperatures over land: regional averages' provide additional information about the consistency of rates for individual seasons.

The question arises of the probability of a particular number of EN and HI events being achieved or exceeded by chance, which provides an estimate of the confidence to be placed in a particular outcome. For contingency tables, the hypergeometric distribution applies and is commonly used to calculate confidence levels, as in Ropelewski and Halpert (1987) for example, and see appendices in Mason and Goddard (2001) for a discussion. Calculation using Monte Carlo simulations of many randomly generated contingency tables is a direct alternative, and the probabilities provided in the following sections were estimated using a 100,000 sample. With reference to Fig. 2, for n = 60, nEN = 15 and nLO = 20 the chance of n(LO and EN) being 7 or more is about 0.17, 8 or more is 0.06 and 9 or more is 0.02. Thus, roughly, 8 or more corresponds to a 5% significance level.

Table 2
Regional temperature statistics for select seasons. For NCEP, 1951–2010 data are used; for CRUTEM the data selection is as in Table 1.

Name	Season	Event	Rate	Rate	Corr(N34,T)	
			NCEP	CRUTEM	NCEP	CRUTEM
NSAmerica	JFM	ENHI + LNLO	22/30 = 0.73	26/30 = 0.87	+0.74	+0.85
CSAmerica	JJA	ENHI + LNLO	17/30 = 0.57	29/50 = 0.58	+0.39	+0.44
SSAmerica	JJA	ENHI + LNLO	18/30 = 0.6	24/50 = 0.48	+0.43	+0.39
MexicoUSA	DJF	ENLO + LNHI	18/30 = 0.6	30/50 = 0.6	−0.32	−0.41
NWNAmerica	MAM	ENHI + LNLO	21/30 = 0.7	31/50 = 0.62	+0.49	+0.55
NENAmerica	JFM	ENHI	9/15 = 0.6	14/25 = 0.56	+0.30	+0.24
	ASO	LNHI	9/15 = 0.6	13/25 = 0.52	−0.34	−0.30
India	SON	ENHI + LNLO	20/30 = 0.67	31/50 = 0.62	+0.44	+0.39
SEAsia	MJJ	ENHI + LNLO	18/30 = 0.6	35/50 = 0.7	+0.34	+0.52
Japan	NDJ	ENHI	10/15 = 0.67	13/25 = 0.52	+0.37	+0.26
	JAS	ENLO + LNHI	19/30 = 0.63	25/50 = 0.5	−0.39	−0.27
Indonesia	DJF	ENHI	10/15 = 0.67	–	+0.40	–
NEAustralia	JFM	ENHI + LNLO	16/30 = 0.53	31/50 = 0.62	+0.50	+0.45
	JAS	ENLO + LNHI	17/30 = 0.57	25/50 = 0.5	−0.46	−0.28
SEAustralia	NDJ	ENHI + LNLO	18/30 = 0.6	28/50 = 0.56	+0.51	+0.43
SWAustralia	OND	ENHI	8/15 = 0.53	15/25 = 0.6	+0.45	+0.35
NewZealand	OND	ENLO + LNHI	20/30 = 0.67	31/50 = 0.62	−0.36	−0.43
NSAfrica	FMA	ENHI + LNLO	18/30 = 0.6	–	+0.43	–
SSAfrica	JFM	ENHI + LNLO	17/30 = 0.57	29/50 = 0.58	+0.56	+0.44
WAfrica	FMA	ENHI	9/15 = 0.6	11/15 = 0.73	+0.52	+0.50
NWAfrica	JFM	ENHI + LNLO	18/30 = 0.6	–	+0.43	–
SEurope	OND	ENHI	9/15 = 0.6	14/25 = 0.56	+0.41	+0.21
NWEurope	JFM	ENLO	5/15 = 0.33	13/25 = 0.52	−0.05	−0.17

As well as the possibility of HI or LO occurring during ENSO conditions, the probability of such categories not occurring is also of interest. In the example in Fig. 2 n(HI and EN) = 2 and the rate of occurrence of HI given EN is 2/15: an estimate of the chance of HI T not occurring when EN conditions prevail is 13/15. As above, the probability of 2 or less HI cases occurring by chance out of 15 EN cases can be found, and is about 0.05: thus one can be 95% confident that the low rate is an EN effect.

Near surface temperatures over land: gridded global maps of rates of occurrence

Maps based on 3 by 3 contingency table information were first generated as described above using the gridded data, treating each location separately. An example for NCEP T over land areas using JFM data for 1951 to 2010 is provided in Fig. 3. As the NCEP T dataset has no missing values, at each location 60 seasonal T values are used with the corresponding seasonal N34 values to generate a contingency table, with nEN = nLN = 15 and nHI = nLO = 20.

The choice of colour scale is related to the probability of various rates arising by chance, which in turn is related to the sample size, as discussed above. In red, orange and yellow areas rates are $8/15 \approx 0.53$ or larger, for which values there is less than 6% probability by chance. In areas with blue shades the rates are $2/15 \approx 0.13$ or less, with less than 5% probability by chance. Locations with ratios from 3/15 to 7/15 are not coloured. With this choice the coloured regions are largely coherent, and we regard these as regions of significant ENSO impact: With a wider range of coloured rates small isolated patches become common on the maps: some of which may be real ENSO impacts, but others arise by chance. Corresponding maps for AMJ, JAS and OND seasons are in Section A of the Supplementary material.

Very few locations have a rate of 0 or 1: occurrence of EN or LN is no guarantee of a particular impact. The largest rates evident in Fig. 3 for JFM occur in northern South America, where HI T occurs very often (and LO T occurs very seldom) in EN conditions, and similarly LO T occurs very often (and HI T very seldom) in LN conditions. In North America similar effects – but with less widespread and less extreme rates – are evident in parts of the northwest, and opposite impacts (LO T in EN, HI T in LN) appear in the region of Mexico and southern USA. In part of the northeast sector EN has a HI T impact, but with no clear LN counterpart.

On the African continent there are HI in EN and LO in LN impacts in southern Africa. In northwest Africa and equatorial east Africa HI T is favoured in EN, with a weaker preference for LO T in LN. In Australia there is a HI in EN plus LO in LN signal in the northeast, and a HI in LN effect in the southeast. In maritime Asia (tropical western Pacific) there is a tendency for HI T in EN, and a less strong tendency for LO T in LN, with similar weaker impacts in India. In north central Asia a tendency for LO T in LN is not matched by an EN impact. Signals in Europe are sparse and weak.

For comparison, the gridded rate maps for JFM constructed using CRUTEM data for the 100 year period 1911–2010 are shown in Fig. 4. (The choice of period is a trade-off between sample size and temporal coverage. The 100 year period is substantially longer than the 60 year NCEP sample, with sufficient data coverage to provide statistics in many regions with ENSO impact. Results are not sensitive to small changes in sample size, and 100 years is a convenient round number for presentation here.) For the CRUTEM dataset the methodology needed to be adapted to deal with missing data. Only locations with temporal coverage above a certain threshold were processed: in the example, the cutoff is 80% coverage. For consistency, the

Table 3
Seasonality and levels of rates of occurrence for regional T, calculated using CRUTEM data as listed in Table 1. The symbol H denotes a rate for HI T between the 'significant' threshold (see text) and 0.6, HH at/ above 0.6, HHH at/above 0.7; HHHH at/above 0.8. Likewise L denotes a rate for LO T between the threshold and 0.6, LL at/above 0.6, LLL at/above 0.7; LLLL at/above 0.8. Significant values in isolated seasons are bracketed ().

Region		Season											
		1 DJF	2 JFM	3 FMA	4 MAM	5 AMJ	6 MJJ	7 JJA	8 JAS	9 ASO	10 SON	11 OND	12 NDJ
NSAmerica	EN	HHHH	HHHH	HHHH	HH	HHH	HH	HH	HH	HHH	H	HH	HHH
	LN	LLL	LLLL	LLLL	LLLL	LLLL	LLL	LLL	LLL	LLL	LLL	LLL	LL
CSAmerica	EN	H	H	H		HH	H	H	HH	H			
	LN		L	LL	L	L	L	LL	L				
SSAmerica	EN			(L)				H	H				
	LN	H		(L)		L	L		(L)		H	H	H
MexicoUSA	EN	LL	LLL	LLL	LL	L			(H)				L
	LN	H	H	H	H	H				(H)		H	H
NWN America	EN	HH	HH	HH	HHH	HH	H	H	H				H
	LN		L	LL	L	LL	L	L	L	L	L	L	
NEN America	EN	H	H							(L)			H
	LN			(L)				H	H	H			
India	EN	H				H	HH	H	H	H	HH	HH	H
	LN		(L)						L	L	LL	LL	L
SEAsia	EN	H	H	H	HH	HHH	HH	HH	H			H	HH
	LN		L	LL	LLL	LLL	LLL	LL	L		LL	LL	LL
Japan	EN			(H)					(L)				(H)
	LN							H	H			(L)	
NE Australia	EN	HH	HH	H	H	H			L	L	L		H
	LN	LL	LL	L						(H)		LL	LL
SE Australia	EN	H	H	H		(H)				H	H	HH	H
	LN	L									L	L	L
SW Australia	EN					H	H	H		H	HH	HH	H
	LN												
New Zealand	EN			(L)				(L)		L	L	LL	
	LN	H				HH	H	H	H	H	H	H	H
WAfrica	EN	(H)		(HHH)				H	H				
	LN							L	LL				
SSAfrica	EN	HH	H	H	H							H	HH
	LN	LL	LL		(L)							LL	LL
SEurope	EN					(L)					HH	H	
	LN												
NW Europe	EN	L	L										
	LN									(H)			

category thresholds for N34 based on all 100 years were applied at each eligible location: thus the selection of EN and LN years is the same for all locations. Category thresholds for HI and LO and contingency tables were then constructed and rates calculated using the available data at each location – so in the example the number of years n considered varies spatially from 80 to 100, but as before at each location nHI = nLO = $n/3$ rounded to the nearest integer. Confidence levels thus vary somewhat from place to place, and for sites of particular interest a more specific analysis should be made. For 100% coverage, nEN = nLN = 25, and nHI = nLO = 33. The random chance of a rate of 12/25 = 0.48 or more is 0.06, and the chance of 5/25 = 0.2 or less is 0.09, and in Fig. 3 the colour scale was chosen to colour rates of more than 0.46 and less than 0.22. Grey areas on the maps in Fig. 4 indicate the land locations with less than 80% temporal data coverage that are excluded from the rates calculations.

The features in Fig. 4 generally match those in Fig. 3. In Fig. 4 most of the northern South America region has less than 80% coverage for the period shown, however in the small area with sufficient data the signal is as in Fig. 3: HI in EN and LO in LN. If coverage of over 90% is selected then overall the result is very similar to Fig. 4, but the small area in northern South America is lost. If the shorter period 1951–2010 is selected then a larger area of northern South America has adequate coverage, with features like those in Fig. 3. Similarly the significant rates prominent in southern Africa in Fig. 3 are sparsely represented in Fig. 4, but the features are enhanced for the 1951–2010 period.

The EN signals in northwestern North America, and EN and LN signals in eastern Australia, are stronger in Fig. 4. Notable differences are the substantial LO during EN signal in NW Europe in Fig. 4 that does not appear in Fig. 3 (this region is exam-

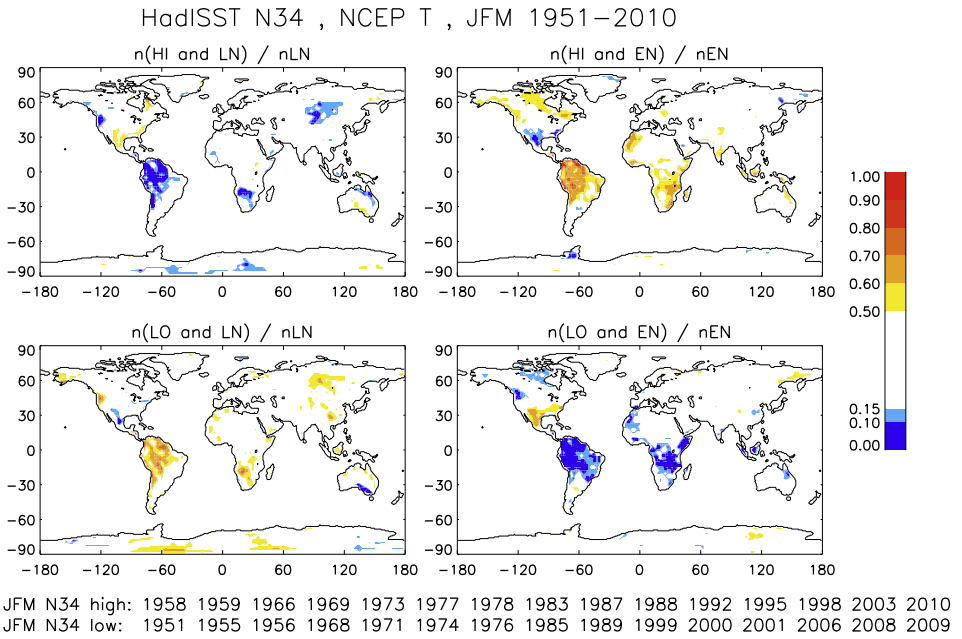

Fig. 3. Rates of occurrence calculated using the Niño3.4 sea surface temperature index and NCEP near-surface T over land areas, for JFM for 1951 to 2010, with nEN = nLN = 15 and nHI = nLO = 20. The top left panel shows the ratio n(HI and LN)/nLN, which is the rate of occurrence of the HI category given the Niño3.4 index in the LN category. Likewise the bottom left panel contains n(LO and LN)/nLN, top right n(HI and EN)/nEN, and bottom right n(LO and EN)/nEN. A list of years for the EN and LN categories is provided below the panels. Locations with rates of 8/15 or more, and 2/15 or less, are coloured. (For interpretation of the references to colour in this figure legend, the reader is referred to the web version of this article.)

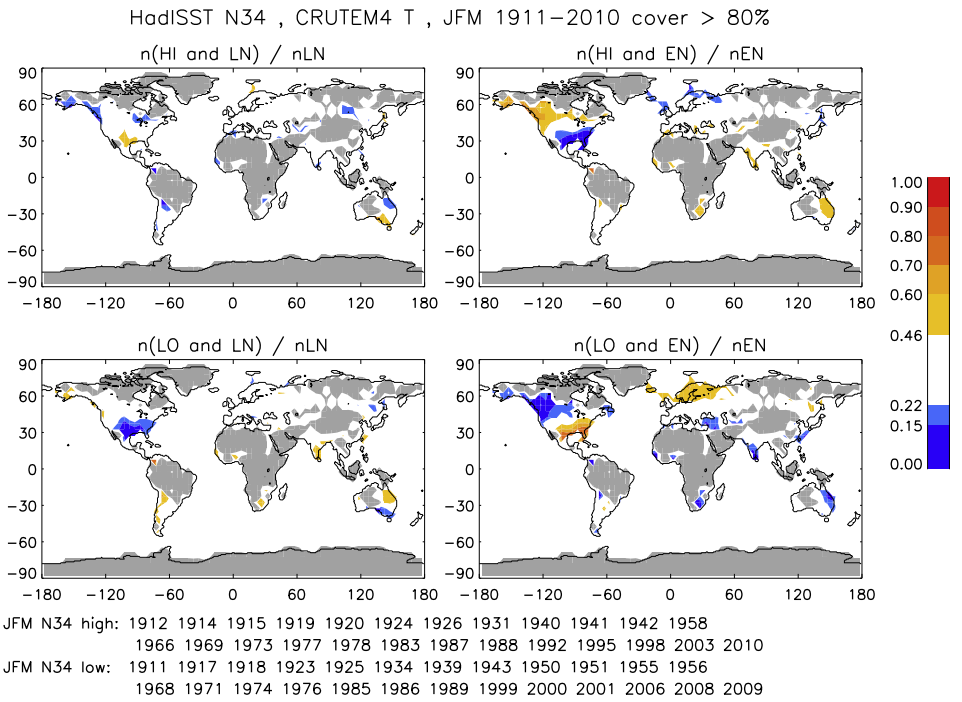

Fig. 4. As Fig. 3, but with rates of occurrence calculated using the Niño3.4 SST index and CRUTEM T over land areas, for JFM for 1911 to 2010. Land areas with temporal coverage below 80% are coloured grey. (The data grid is relatively coarse, so the drawn coastlines do not match the data exactly.). (For interpretation of the references to colour in this figure legend, the reader is referred to the web version of this article.)

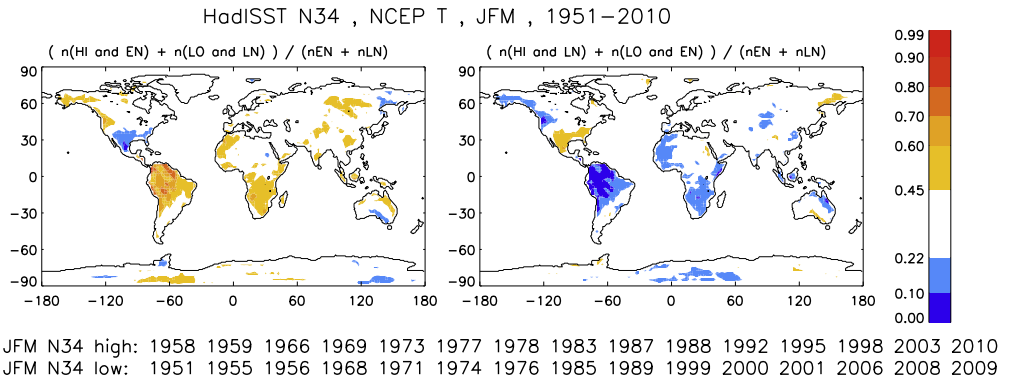

Fig. 5. Maps of rates of occurrence for combined EN and LN events, using NCEP T 1951–2010, for the JFM season. Locations with rates 14/30 or more, or 6/30 or less, are coloured. (For interpretation of the references to colour in this figure legend, the reader is referred to the web version of this article.)

ined further in Section 'Near surface temperatures over land: regional averages'), and the absence of a central Asia feature in Fig. 4.

As documented in previous analyses, there is a high level of symmetry in ENSO effects, in that e.g. high rates for HI in EN are mirrored by high rates for LO in LN. Indeed, analyses are often designed to investigate combined effects, using for example composite differences or linear regression statistics. The combined effects of EN and LN can similarly be assessed here by adding contingency table entries to calculate combined rates of occurrence as the ratios $(n(\text{HI and EN}) + n(\text{LO and LN}))/(n\text{EN} + n\text{LN})$ and $(n(\text{LO and EN}) + n(\text{HI and LN}))/(n\text{EN} + n\text{LN})$. The result corresponding to Fig. 3 for JFM 1951–2010 for NCEP T data is provided in Fig. 5. With $n\text{EN} + n\text{LN} = 30$, a rate of $14/30 \approx 0.47$ or more has a chance 0.08, and a rate of $6/30 = 0.2$ or less has a chance of 0.07. Thus locations with rates 14/30 or more, or 6/30 or less, are coloured in Fig. 5.

Where a high rate occurs in one panel in Fig. 5 it is usually accompanied by a low rate in the other panel. While the combined rates serve to enhance some features, it should be noted that areas that appear significant in the 'composite' view do not necessarily arise in the separate EN and LN components. For example, in central Asia rates for 'HI in EN and LO in LN' are prominent in Fig. 5, but only LO in LN appears significant in Fig. 3. (Note that central Asia also does not feature in Fig. 4.) Similarly, a region that does not seem significant in the 'composite' may have a significant component: e.g. in Fig. 3 rates for HI given EN are significant in parts of northeast North America, but in that region the rates for LO given LN are not significant, and the rates for 'HI in EN and LO in LN' are not significant in Fig. 5.

Features in Fig. 5 mainly correspond to those identified in previous studies using different measures: see e.g. panel 'DJF+1' in Figs. 2 and 4 of Kiladis and Diaz (1989), in which EN and LN effects are combined in composites. (In Kiladis and Diaz (1989) the central Asia signal again does not appear.)

The asymmetry in parts of North America in Figs. 3 and 4 is also evident in other analyses, and is investigated further in Section 'Near surface temperatures over land: regional averages'. Hoerling et al. (1997) provided evidence that this contrast in EN and LN teleconnections is associated with a phase difference between the atmospheric wavetrains induced by EN compared to LN events, in turn associated with differences in the location of the tropical Pacific rainfall anomalies that drive the wavetrains.

Gridded global maps of rates of occurrence for sea surface temperature

As is well known, SST variability in a large proportion of the world's oceans is influenced by ENSO. Complementary to the land T analysis, the same contingency table methodology was applied to sea surface temperature using the gridded HadISST dataset, choosing 1951–2010 to match Fig. 3. The resulting maps of rates of occurrence are provided for JFM in Fig. 6, with a Pacific-centred viewpoint.

Patterns are similar to those obtained using composites of EN and LN events (see e.g. Fig. 1 in Hoerling et al., 1997). There is again a high degree of symmetry between EN and LN. For EN, in the tropical Pacific the high rates of occurrence of HI SST in the broad central-east equatorial region extend northward along the North American coastal region, and are accompanied by a horseshoe pattern of LO SST in the west and subtropical Pacific, which in the southern Pacific has a branch extending across New Zealand. The horseshoe does not extend to the Asian coast. For EN there are high rates for HI SST (and similarly high rates for LO in LN) over much of the Indian ocean, with moderate rates extending into the Pacific near the Asian coast for EN conditions. In the tropical Atlantic during EN moderate to high rates appear between the equator and 30S, and near 15N in the west. In the north Atlantic there is a weaker preference for LO SST along a line from Florida to Ireland. In LN conditions HI SST is favoured in the central north Atlantic. In the Southern Ocean during EN, HI is favoured in the Pacific and Indian sectors but LO in the Atlantic, with opposite tendencies in LN conditions. The impacts on SST are associated with ENSO-induced atmospheric changes, and help to maintain impacts in land areas through further ocean–atmosphere interactions.

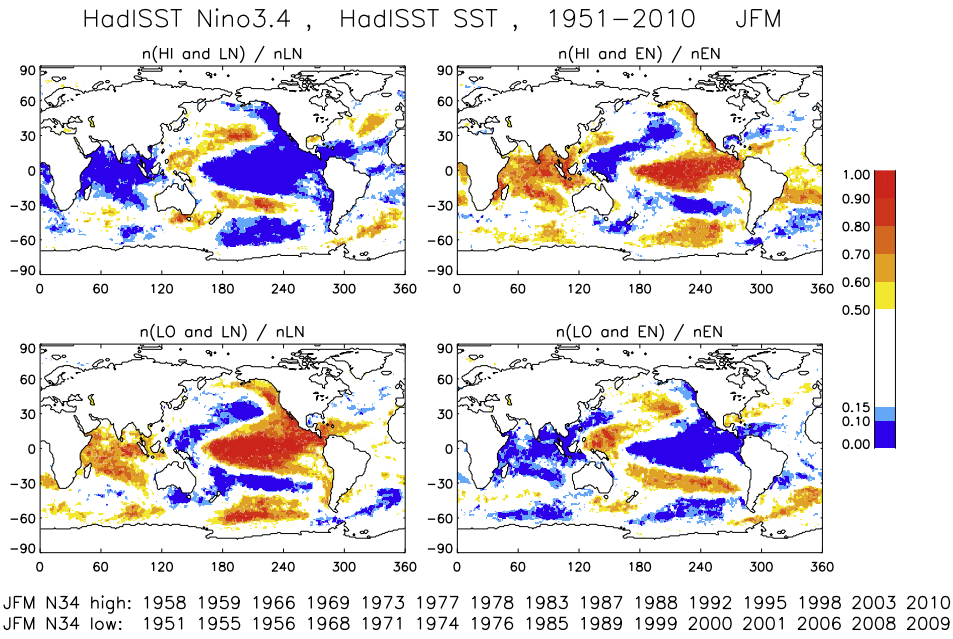

Fig. 6. Cf Fig. 3: maps of rates of occurrence for the JFM season calculated using the Niño3.4 index and HadISST sea surface temperature for 1951–2010.

Near surface temperatures over land: regional averages

From the gridded seasonal maps of rates of occurrence several regions with substantial impact are evident. To investigate these further, several regions were defined as in Table 1. (The region names are just indicative. Location maps are provided in Section C of the Supplementary material.) The regional averages were calculated as follows: at each land point within the region and for each season standardised anomalies were calculated, then these values were averaged over the region. (For CRUTEM, averages were constructed using land gridpoints with temporal coverage above some threshold, as indicated in Table 1.) Using the regional averages and N34 data, 3 by 3 contingency tables and associated rates of occurrence were constructed for each season as before. The regions were selected to provide examples of the main impacts and seasonal cycles emerging from the rates of occurrence data. Note that significant impacts also occur beyond the regional boundaries: for example the NENAmerica region represents the overlapping portion of larger areas with diverse impacts. Further, the selected regions are fixed year-round, and with the shift of impacts with season some impacts are not represented fully.

An example of the seasonality of regional ENSO impacts is provided in Fig. 7, which shows the seasonal dependence of the rates of occurrence (including combined rates) and of the correlation between the N34 and regional T timeseries. As is typical of all the regions considered, there is a clear seasonal cycle to be seen.

NENAmerica was selected as an example of a region where impacts reverse during the seasonal cycle. (It is also a region with excellent data coverage.) During EN conditions the 'significant' rate of 12/25 for HI T is reached in seasons 12,1,2 (NDJ, DJF, JFM), whereas LO T is favoured in the third quarter of the year. During LN conditions the 12/25 rate for HI T is reached in seasons 7, 8 and 9: however rates for LO T are well below this threshold all year. To put it another way, HI T can be expected in both EN and LN conditions, but at different times of year. For the combined rates of occurrence, that for 'LO in EN and HI in LN' reaches the 22/50 rate in seasons 7–9; and that for 'HI in EN and LO in LN' reaches 22/50 in seasons 1–3. In this extratropical region the rates of occurrence are not particularly high, all being below 60%. The correlation between the N34 and T timeseries for each season is included in Fig. 7. The sign of the correlation changes during the year: it is larger than 0.2 in seasons 1 and 2, but less than −0.2 in seasons 7–9. Similar reversal in this region is evident in, for example, the regression maps in Yang and DelSole (2012) for DJF and JAS.

In Table 2 rates of occurrence and correlation statistics for select seasons are provided for the regions in Table 1. For comparison, statistics are provided for NCEP (1951–2010) and CRUTEM (data as in Table 1: note insufficient coverage for CRUTEM in NSAfrica and Indonesia regions). For most examples the impact is largely symmetric (e.g. HI during EN is accompanied by LO during LN for the same season, both having rates of occurrence that reach threshold levels), and for these cases the rates for combined events (denoted ENHI + LNLO or ENLO + LNHI) are provided in Table 2. The anomaly correlations between N34 and the regionally-averaged T for the relevant seasons are included.

Note that depending on season and region the CRUTEM and NCEP regionally averaged T data can differ substantially. For example, comparing data in 1951–2010, the correlation between CRUTEM and NCEP regional T timeseries is 0.92 for NENAmerica JJA, but 0.71 for SSAfrica JJA where data coverage is less complete. The differences are sufficient for categorisations to differ somewhat, but generally the overall picture of impact and seasonality is consistent.

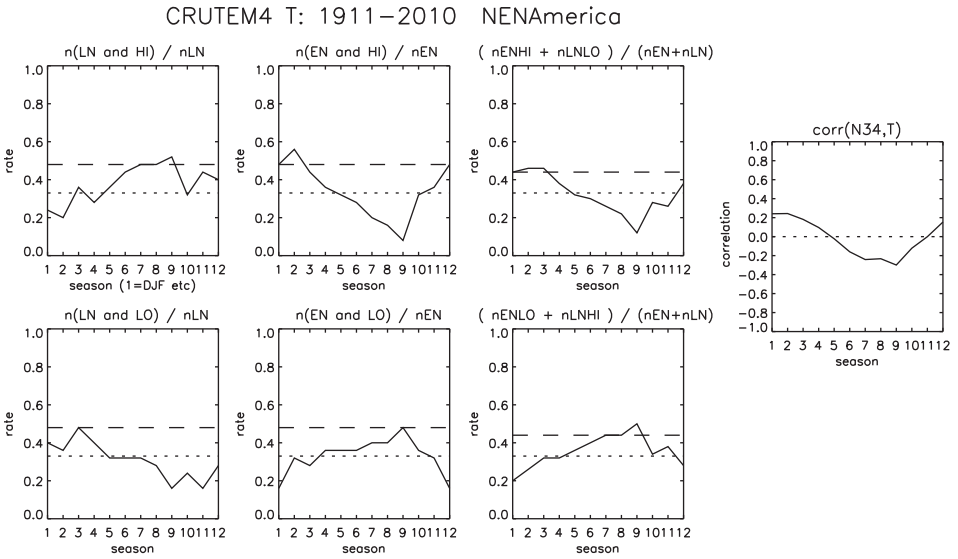

Fig. 7. The seasonal cycle of the rates of occurrence and of the anomaly correlation (N34,T) for the NENAmerica region (45N–55N, 270E–295E), calculated using the Niño3.4 index and CRUTEM T for 1911–2010. Rates of occurrence are provided for LN and HI (top left), LN and LO (bottom left), EN and HI (top centre), and EN and LO (bottom centre). Combined rates are on the right, and correlation on the far right. For the rates, the dotted line indicates the climatological chance 0.33, and the dashed line indicates the 'significant' value (see text). For the correlation panel, the zero line is dotted.

For most regions, there is good agreement in Table 2 for the statistics from different datasets and periods. The most obvious difference is in NWEurope, where impact is relatively low: this is the only region where correlations have magnitude below 0.2 in the select seasons, and it is described in more detail below.

Generally moderate (magnitude larger than about 0.25) to high correlations give some indication of when to expect significant rates of occurrence, but the impact may not be symmetric between EN and LN. Note that in Fig. 7 correlations are over 0.25 in seasons 1 and 2, but this is associated with HI given EN impact and there is no LO given LN impact.

In some regions there is significant impact over several seasons, while in others significant impact is confined to a few months. In Table 3 the seasonality and levels of rates of occurrence are indicated for the select regions, using results calculated with CRUTEM data for years and coverage as in Table 1: similar results are obtained with the NCEP data.

The region with the highest impact according to the rate of occurrence measure is NSAmerica, where rates are both highest (reaching over 0.8 for HI in EN conditions and LO in LN) and most extensive seasonally, being 'significant' all year for both EN and LN, with highest rates in JFM.

In CSAmerica rates are significant most of the year, and largest in austral winter. Impacts are reduced in SSAmerica, with weak but significant HI in EN and LO in LN signals in the austral summer. For DJF only, there is a weak reversed impact. (This 'reversed' effect also appears in Fig. 4 of Kiladis and Diaz, 1989.)

Within North America, in MexicoUSA there is a moderate to strong LO in EN and HI in LN impact in seasons 1–4: this is the region with the largest LO in EN and HI in LN impact. In NWNAmerica rates for HI in EN are moderate to strong in seasons 1–5. By contrast the rates for LO in LN are weaker, with significant levels scattered through seasons 2,3, 5,6 and 9–11. This asymmetry is more pronounced in NENAmerica, with weak HI in EN rates in boreal winter and HI in LN in seasons 7–9.

In Asia impacts are evident in the India region, where in Table 3 HI in EN is favoured in seasons 5–12,1 with highest rates in seasons 10 and 11, and similarly impact for LO in LN is again highest in seasons 10 and 11. In the SEAsia region impacts are stronger, with significant HI in EN and LO in LN rates nearly all year, and moderate to strong levels in seasons 4–7. In Indonesia HI in EN is favoured in seasons 11,12,1,2. By contrast, in Japan the clearest impact is HI in LN in JAS, with a weaker LO in LN rate in that season. Here there is also a tendency for impact reversal, with indications of HI in EN in seasons 3 and 12, and LO in LN in season 11.

Seasonal reversal is also evident in NEAustralia, where there are significant weak to moderate rates for HI in EN and LO in LN in seasons 12,1–3, and a less pronounced preference for LO in EN and HI in LN in austral late winter/early spring. In New Zealand HI in LN is favoured most of the year, with a LO in EN impact that is less extensive, being more evident in months 9–11.

In the African continent impacts are most evident in southern Africa: in the SSAfrica region there is weak to moderate HI in EN impact in seasons 11,12,1–4, and corresponding moderate LO in LN rates in seasons 11,12,1,2. (In NSAfrica the same impact occurs, shifted later in the year, based on NCEP data, not shown.) In WAfrica there are two periods, the first and third quarters of the year, that have an ENSO impact that favours HI in EN and LO in LN. In CRUTEM the signal in the third quarter is more consistent, whereas in NCEP data the first quarter is more evident. In NWAfrica, rates for both HI in EN and LO in LN

are significant in seasons 1 and 2. In this region the correlation between N34 and T reverses during the seasonal cycle, and in seasons 7 and 8 LO in EN is favoured, along with some indication of HI in LN in season 9.

Within Europe, although there is other evidence for ENSO effects in several sectors (see e.g. the schematic Fig. 17 in Brönnimann, 2007, and Fig. 2 in Kiladis and Diaz, 1989), in the rate of occurrence analysis for T there are few significant signals, confined to NWEurope with LO T in EN in boreal winter, and SEurope with HI in EN in seasons 10 and 11.

In the above summary there are examples of regions with impacts that in a sense reverse during the seasonal cycle (NEAustralia, Japan, NENAmerica and NWAfrica), which are characterised also by correlations between T and N34 that have positive and negative stages during the year. This behaviour can also be seen in the regression maps in Yang and DelSole (2012). (As the regressions in Yang and DelSole (2012) were calculated using NCEP T, the correlation behaviour in Table 2 is generally similar to their results.) There are also very low rates in some regions and seasons, signifying a low chance of, say, HI T occurring in LN conditions etc. Details are not provided in this overview, but this is an aspect that a specific regional analysis should include.

Northwest Europe

Further investigation of NWEurope is provided here. For LO T in EN conditions in JFM the rates in the NWEurope region appear significant in Fig. 4 (CRUTEM), but markedly less so in Fig. 3 (NCEP). This is a region of very good data coverage in CRUTEM: in the 1911–2010 period most locations in the region in the gridded dataset have 100% temporal coverage. The scatterplot and contingency table for this period are shown in Fig. 8.

A feature that stands out in Fig. 8 is that while there is overall a preference for LO T in EN conditions (ratio 13/25), for high N34 temperatures (notably 1983 and 1998, and also third-highest 1992) the outcome was HI T. In the latter half of the 20th century the 1982/83 and 1997/98 EN events were exceptionally strong (see Fig. 1), and NWEurope is a region where impacts during these events that were contrary to the 'usual' effect are particularly evident. (Note that in Fig. 2 the impacts in the years marked 83 and 98 are also contrary.) Toniazzo and Scaife (2006) stratify EN events by amplitude and find a non-linear yet robust response in late winter that changes sign as the amplitude of the EN anomaly increases. The pressure pattern associated with the majority of EN events is the well-documented negative NAO-like pattern (Moron and Gouirand, 2003) that is associated with cold temperatures over northern Europe (Brönnimann et al., 2007). For the largest EN events the pattern is rather different, with high pressure to the west of the UK. Different teleconnection pathways have been identified for the two responses with an active stratosphere playing a key role for the response in moderate EN events and a tropospheric pathway via the Atlantic suggested for the strongest events (see Toniazzo and Scaife, 2006; Bell et al., 2009).

Another factor is the effect of major volcanic eruptions, particularly in the tropics (Agung March 1963, El Chichon April 1982, Pinatubo June 1991), which can be substantial and last several seasons. There are regional and seasonal variations: e.g. an overall tendency to cool T in following seasons is contrasted by a winter warming effect over northern hemisphere extratropical continents; see for example Fig. 7 in the review by Robock (2000) which shows winter warming in NWEurope after Pinatubo. Volcanic effects likely contribute to the placement of points 83 and 92 in the HI category in Fig. 8. In Fig. 3 of Brönnimann (2007) linear regression maps of T and PR versus N34 for seasons during ENSO events are provided, with the two winters following tropical eruptions removed.

Major EN events and volcanic eruptions are rare, and from the point of view of attribution of effects, it is a difficulty that they sometimes coincide! In the rate of occurrence analysis they do not appear to have a large influence on the results presented here: however for specific applications such effects should be considered.

NWEurope is also a region where the rate of occurrence analysis is particularly sensitive to the assessment period. Although the JFM rate for LO in EN is significant for CRUTEM 1911–2010, for CRUTEM 1951–2010 the rate is 5/15, in agreement with the NCEP result in Table 2, with no evidence of an EN impact.

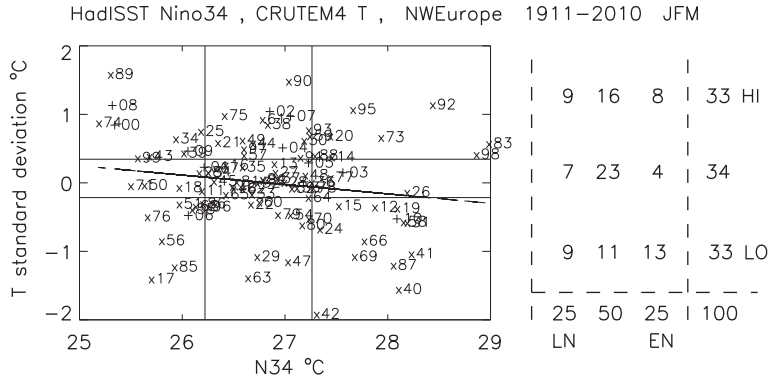

Fig. 8. Cf Fig. 2: scatterplot and contingency table for the JFM season for the Niño3.4 index and NWEurope T (50N–70N, 5E–45E) from CRUTEM, for 1911–2010.

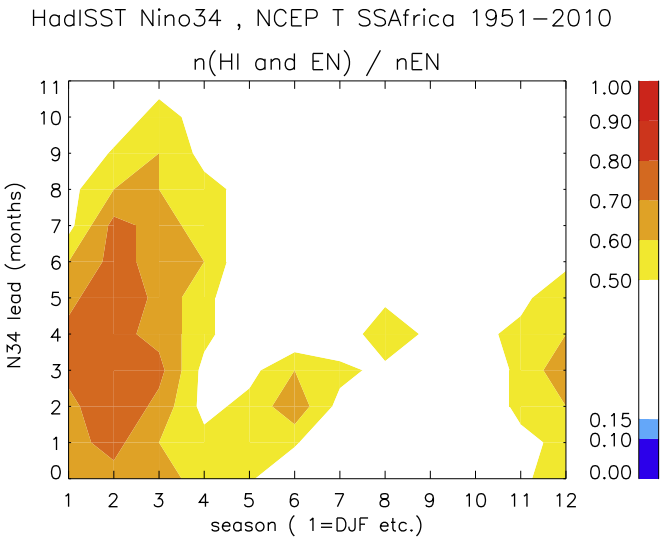

Fig. 9. Rates of occurrence for HI T in EN, for the SSAfrica region calculated using seasonal N34 values for 0–11 months ahead of the regional T values for each calendar season. Thus values along the 'season' axis at lead 0 are contemporary, while others have N34 leading. Rates were calculated using NCEP T 1951–2010.

Time lagged impacts

The results described above use contemporary N34 and T values. As ENSO events typically last several months, results are generally very similar if neighbouring N34 seasons are used in analysing a particular region and season. However there is the possibility that significant T impacts that lag N34 (e.g. effects that become evident regionally after an event declines as defined by N34) could be overlooked in the contemporary analysis, so an investigation of lag effects was carried out.

An example is provided in Fig. 9, which shows rates of occurrence for HI T given EN conditions for the SSAfrica region, with N34 leading up to 11 months ahead of each regional season. The main feature is that the contemporary signal of significant moderate rates in the first quarter is also evident for N34 leading by up to about 6 months. In this example there is also some modest sign of seasonal impacts that are not picked up by contemporary statistics, with significant rates in MJJ at a lead of 2 months that extend the contemporary period of moderate rates.

In other regions examined the main features were likewise significant rates for N34 leading the seasons with contemporary significant rates by several months. This reflects the importance of ENSO as a major predictive factor in seasonal climate. We did not find evidence of substantial lagged impacts that were not 'connected' to contemporary impacts. Nevertheless, the possibility of separate lagged impacts should be included in more detailed analyses for particular applications.

Gridded global maps of rates of occurrence for precipitation

Using the GPCP and CMAP precipitation datasets, rates of occurrence were calculated using the same procedure as for the T maps. The rate maps for the October–November–December season, using GPCP 1979–2012 data, are provided in Fig. 10. With n = 34 years nEN = nLN = 9, and nHI = nLO = 11. The random chance of a rate of 5 or more out of 9 is about 0.09, and of 6 or more is 0.02. The chance of 0/9 is 0.02, and of 1/9 or less is 0.12. We opted to colour rates at and above 5/9, and at or below 1/9 to provide an impression of the pattern of impacts. Rates for land and sea are shown, with a Pacific-centred view.

The main impact is in the Pacific sector, where rates are high in the central and west equatorial Pacific, reflecting the displacement eastward (westward) of convergence zones during EN (LN) events. The main evident land impacts in OND are in South America and Australasia. The patterns are largely symmetric between EN and LN. Over the land rates for PR are generally lower than those found for T, rarely exceeding 0.7. Corresponding maps for JFM, AMJ and JAS seasons are provided in Section B of the Supplementary material.

The features in Fig. 10 can be compared with the SON rate maps in Figs. 4 and 8 in Mason and Goddard (2001): note that areas where rainfall is seasonally low are shaded out in Mason and Goddard (2001). Features in common are LO PR in EN and HI PR in LN in northern South America, southeast Australia, maritime Asia; HI in EN and LO in LN in southern South America and southern Africa; HI in EN in equatorial east Africa and southwest USA. Similar features appear in Kiladis and Diaz (1989), Figs. 3 and 5, in the panels marked SON 0 (i.e. composites for the September–October–November seasons, using years in which ENSO peaks).

There are also points of contrast: the signal for LO in EN and HI in LN is prominent in India in Mason and Goddard (2001), but not in Fig. 10 – here the slight shift in season (SON vs OND) makes some difference: see Table 6 and Fig. 11 below. For

southwest Europe a signal for HI in EN and LO in LN is evident in Mason and Goddard (2001), but not in Fig. 10. In this case rates in this region reach significant levels when regional averages are calculated: see Tables 5 and 6 below. In the Sahel region there is a tendency for LO in EN and HI in LN in Mason and Goddard (2001), but a tendency for HI in EN in Fig. 10. In our analysis the LO in EN and HI in LN signal is found in mid-year when seasonal rainfall is largest (as in other studies), but with a tendency to reverse by the end of the year (see Table 6).

Precipitation regional averages

Rates of occurrence are increased by regional averaging, and the regions defined in Table 4 were selected to provide examples of the locations and seasonality of the main impacts. (A map of the locations is provided in Section C of the Supplementary material.) Seasonal data were averaged using grid points over land within the defined regions, except for the Sri Lanka, Philippines and Indonesia regions where points over land and ocean were used. Note that although the same names are used for some T and PR regions, the geographic details differ somewhat. As before, where used, country names for regions indicate the largest country within the region which may also contain parts of nearby countries.

In most regions the GPCP and CMAP regionally averaged PR values are closely similar (temporal correlation over 0.9), but in the WSAmerica and Caribbean regions there are more substantial differences with correlations below 0.7 in some seasons.

An example of the seasonal cycle of rates of occurrence is provided in Fig. 11, for the India region. In the monsoon season in the middle of the year rates are at/above the significant 5/9 level for LO given EN conditions, reaching 7/9 in JJA: notably

Table 4
Regions defined to calculate seasonal area-averaged precipitation, using data at land points, except for those marked LS where land and sea points were used.

Name	Location	Name	Location
NSAmerica	2N–12N, 77W–52W	WSAmerica	10S–0, 82W–75W
NEBrazil	10S–5S, 42W–34W	SSAmerica	45S–30S, 70W–53W
MexUSA	30N–35N, 120W–90W	NWUSA	40N–50N, 125W–108W
NEUSA	40N–50N, 90W–77W	SEUSA	25N–35N, 90W–78W
Caribbean	15N–25N, 83W–68W	India	12N–28N, 70E–83E
SriLanka	5N–10N, 80E–83E (LS)	EChina	20N–30N, 105E–120E
SEAsia	5–20N, 95E–110E	Philippines	5N–20N, 120E–127E (LS)
Indonesia	10S–5N, 100E–130E (LS)	NEAustralia	28S–10S, 135E–155E
SEAustralia	40S–30S, 140E–155E	SWAustralia	35S–30S, 115E–125E
EAfrica	5S–5N, 35E–45E	Sahel	10N–15N, 15W–40E
SSAfrica	28S–18S, 18E–33E	SWEurope	37N–47N, 10W–5E

Abbreviations used for the regional names are, for example, NSAmerica for northern South America, SEAsia for south-east Asia.

Table 5
Regional precipitation statistics for select seasons, using GPCP 1979–2012 and CMAP 1979–2010 data.

Name	Season	Event	Rate	Rate	Corr(N34,PR)	
			GPCP	CMAP	GPCP	CMAP
NSAmerica	NDJ	ENLO + LNHI	15/18 = 0.83	11/16 = 0.69	−0.81	−0.70
WSAmerica	JFM	ENLO + LNHI	12/18 = 0.67	10/16 = 0.62	−0.26	−0.34
NEBrazil	FMA	ENLO + LNHI	11/18 = 0.61	12/16 = 0.75	−0.53	−0.56
SSAmerica	OND	ENHI + LNLO	13/18 = 0.72	10/16 = 0.56	+0.64	+0.64
MexUSA	OND	ENHI	6/9 = 0.67	5/8 = 0.62	+0.40	+0.37
NWUSA	OND	ENLO + LNHI	10/18 = 0.56	9/16 = 0.56	−0.23	−0.18
NEUSA	MAM	ENLO	5/9 = 0.56	4/8 = 0.50	−0.08	+0.03
SEUSA	DJF	ENHI + LNLO	11/18 = 0.61	9/16 = 0.50	+0.61	+0.54
Caribbean	JFM	LNLO	6/9 = 0.67	3/8 = 0.38	+0.50	+0.46
	ASO	ENLO	7/9 = 0.78	4/8 = 0.50	−0.44	−0.37
India	JAS	ENLO + LNHI	10/18 = 0.56	8/16 = 0.50	−0.45	−0.35
SriLanka	JFM	LNHI	6/9 = 0.67	5/8 = 0.62	−0.57	−0.46
EChina	MJJ	LNLO	6/9 = 0.67	4/8 = 0.50	+0.32	+0.22
SEAsia	MAM	ENLO + LNHI	12/18 = 0.67	12/16 = 0.75	−0.79	−0.78
Philippines	OND	ENLO + LNHI	14/18 = 0.78	14/16 = 0.87	−0.84	−0.85
Indonesia	FMA	ENLO + LNHI	14/18 = 0.78	12/16 = 0.75	−0.72	−0.76
NEAustralia	NDJ	ENLO + LNHI	13/18 = 0.72	12/16 = 0.75	−0.45	−0.49
SEAustralia	OND	ENLO + LNHI	12/18 = 0.67	11/16 = 0.69	−0.57	−0.59
SWAustralia	DJF	LNHI	7/9 = 0.78	6/8 = 0.75	−0.48	−0.45
EAfrica	OND	ENHI	6/9 = 0.67	5/8 = 0.62	+0.51	+0.58
Sahel	JAS	ENLO + LNHI	9/18 = 0.5	12/16 = 0.75	−0.35	−0.43
SSAfrica	DJF	ENLO + LNHI	13/18 = 0.72	12/16 = 0.75	−0.60	−0.62
SWEurope	SON	ENHI + LNLO	12/18 = 0.67	11/16 = 0.69	+0.44	0.45

Table 6
Seasonal rates of occurrence for regional precipitation during EN and LN events, from GPCP 1979–2012 data. The symbol H denotes a rate of 5/9 for HI PR, HH denotes 6/9, HHH 7/9, HHHH 8/9. Likewise the rate for LO PR is denoted by L for 5/9, LL 6/9, LLL 7/9, LLLL 8/9, LLLLL 9/9. Values in isolated seasons are marked (). Seasons for which climatological precipitation is largest are shaded.

Region	Event	Season											
		1 DJF	2 JFM	3 FMA	4 MAM	5 AMJ	6 MJJ	7 JJA	8 JAS	9 ASO	10 SON	11 OND	12 NDJ
NSAmerica	EN	LLL	LLL				L	L	L		L	LL	LLLLL
	LN	HHH	HHH		L	L			H	H	H	HHH	HH
WSAmerica	EN		L	L						H	H		
	LN		HHH	HHH			(H)			(L)			
NEBrazil	EN			L	L	L							
	LN			HH	HH	HH	HH	H	H				
SSAmerica	EN	HH				HH	H	H				HH	H
	LN			(LL)								LLL	LL
MexUSA	EN	HH		(H)								HH	HH
	LN	(L)		(L)							(L)		
NWUSA	EN				(H)			(H)				(L)	
	LN					(L)						(H)	
NEUSA	EN	L	L		L	L				L	L		
	LN	(H)					(H)					(H)	
SEUSA	EN	H									H	HH	H
	LN	LL	LL		L	L							LL
Caribbean	EN			(HH)				LL	L	LLL	LL	L	
	LN	L	LL						(H)				L
SEAsia	EN			LL	LLLL	LLL	LL		(H)			(L)	
	LN	HH	HHH	HHH		(HH)			(L)	H	H	HH	
India	EN			(L)		L	LL	LLL	L	L			(HH)
	LN	L							H	H	H		LL
SriLanka	EN			(L)						(HH)			
	LN		HH	H				(HH)			(L)		
EChina	EN	HH			(H)							H	HHH
	LN				(L)		LL	L		(H)			(L)
Philippines	EN	LL	LLL	LLL	LLL	LLL	LL			LL	LLL	LL	LL
	LN	HHHH	HHH	HHH	HH	H				HH	H	HHHH	HHH
Indonesia	EN	L	L	LLL	LL	L	LL	LLLL	LLL	LLLL	LLLL	LLL	LLL
	LN	HH	H	HHH	HHH		HH	HH		HH	HH	H	H
NEAustralia	EN					L	L	LL	LL	LL	LL	LL	LL
	LN			H	H			(H)		H	H	H	HHH
SEAustralia	EN			(H)					L	L	LL	LL	
	LN				(H)					H	HH	HH	HH
SWAustralia	EN	L	L						(L)				
	LN	HHH		HH	H	H						H	H
EAfrica	EN	H								H	HH	HH	HH
	LN	(L)					(L)						
Sahel	EN							L	L		H	H	
	LN				L	L			H	H			
SSAfrica	EN	LLL	L	L						(H)		L	L
	LN	HH	H		H	H	H					(HH)	
SWEurope	EN				(L)				H	H	HH	H	
	LN	(L)			(H)					LL	LL	L	

rates for HI given EN are 0 for AMJ and JJA. Rates for HI given LN are lower, and just reach 5/9 for the latter half of the monsoon. Also notable is the reversal of the relationships in boreal winter, as reflected in the correlation seasonal cycle in Fig. 11: however for this region this occurs when climatological rainfall is very low and when there is little difference between HI and LO category boundaries.

Statistics of rates and correlations for selected seasons are provided in Table 5, based on GPCP 1979–2012 and CMAP 1979–2010 data. Where both 'HI during EN' and 'LO during LN' rates are significant (and vice versa), combined rates are provided: cf Table 2. In Table 6 the seasonality and level of impact are indicated for each region, based on GPCP 1979–2012 data: the season with largest climatological rainfall is shaded.

As would be expected given the similarity of the data sources, results from GPCP and CMAP in Table 5 are in good agreement. In Table 6 a rate of 9/9 appears for one region and season and event: LO in EN for NDJ in NSAmerica. In this region rates for LO in EN and HI in LN are high in seasons 11,12,1,2. (Climatologically, rainfall is relatively low at that time of year, but still about 50% of the maximum.) During seasons 6–8 rates for LO in EN are significant but weaker.

In SSAmerica the behaviour is opposite to NSAmerica, in that HI in EN and/or LO in LN is moderately favoured in seasons 11 and 12, and HI in EN is favoured in seasons 5–7. In central SAmerica the situation is more complex. In NEBrazil moderate rates for HI in LN are found in seasons 3–6, and a lesser impact for LO in EN in seasons 3–5. (This is a region where the rela-

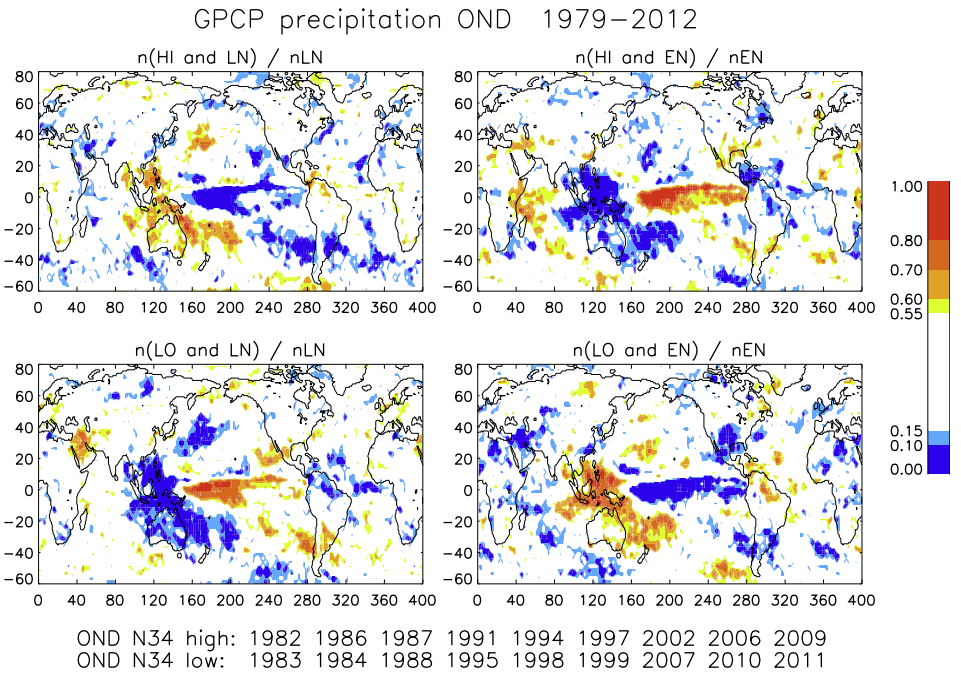

Fig. 10. Cf Fig. 3: rates of occurrence from contingency tables calculated using the Niño3.4 sea surface temperature index and GPCP PR, for October–November–December for 1979–2012. Locations with rates of 5/9 or more, and 1/9 or less, are coloured. (For interpretation of the references to colour in this figure legend, the reader is referred to the web version of this article.)

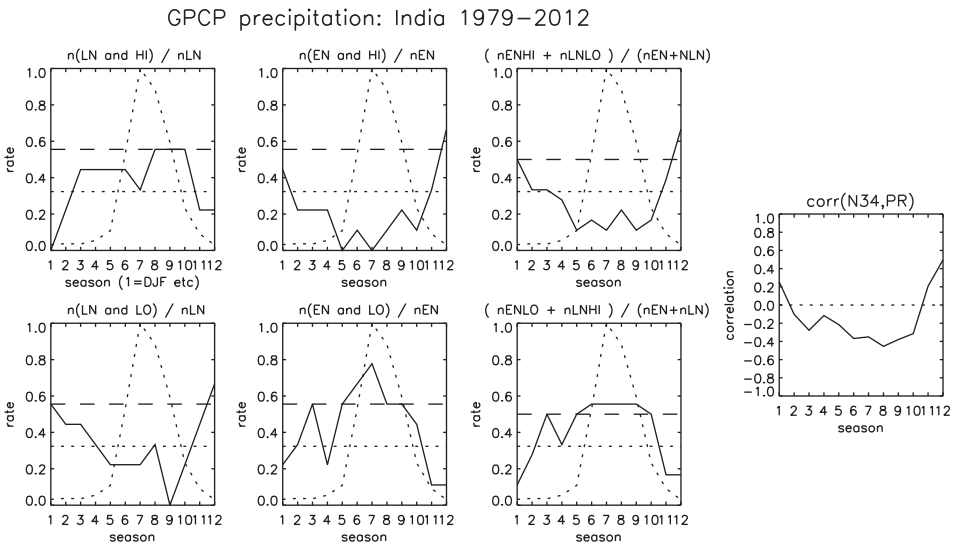

Fig. 11. Cf Fig. 7: the seasonal cycle of rates of occurrence and correlation (N34,T) for the India region (12N–28N, 70E–83E). The dotted curve is the climatological seasonal cycle of monthly precipitation, scaled by the maximum of 9.2 mm/day. On the rate panels the horizontal dashed line indicates the significant rate, while the horizontal dotted line is the climatological chance.

tion between ENSO and rainfall is an important factor in the statistical long-range forecasts initiated in the 1980s by the Met Office: see Folland et al. (2001).) In WSAmerica similarly there is a high rate for HI in LN and a weaker LO in EN rate in seasons 2 and 3, but an opposite tendency in seasons 9 and 10, with a reversal in the seasonal cycle of the correlation between N34 and PR (not shown): indeed this regional average covers an area where larger regions with opposite tendencies in different seasons overlap.

In the MexUSA region (which here includes SWUSA but not SEUSA) there are moderate rates for HI in EN in seasons 11,12, and 1, with a weaker and less consistent signal for LO in LN. In NWUSA there are weak and erratic tendencies for HI in EN and

LO in LN in the second quarter of the year, and an opposite tendency in OND. (Again, this is a region with reversal of the correlation between N34 and PR: +0.34 in MJJ and −0.23 in OND.) In NEUSA rates are erratic, and the only season with significant rates for both LO in EN and HI in LN is DJF; however rates for LO in EN are at or near significant levels in most seasons.

In SEUSA behaviour is similar to that in MexUSA, but with a stronger signal for LO in LN in seasons 12,1,2. To the south in the Caribbean there is again a tendency for LO in LN in seasons 12,1,2, but by contrast moderate to strong rates for LO in EN within seasons 7–10.

As noted above for Fig. 11, the main signal in the India region is for LO in EN in the monsoon season. Separate attention is given to Sri Lanka as impacts there are different, being mainly a tendency for HI in LN in seasons 2 and 3, and some indication of HI in EN in ASO (opposite to the impact in the India region in that season: this behaviour also appears in Kiladis and Diaz (1989), Fig. 3 panel SON 0). In Sri Lanka there is a reversal of seasonal N34 versus PR correlation between FMA (−0.64) and SON (+0.36), and also a substantial semiannual component in the seasonal cycle of rates and correlations. In EChina moderate to strong rates for HI in EN occur in seasons 12 and 1. The climatological rainfall peak here is in boreal summer, when there is a moderate LO in LN impact in the GPCP data.

Closer to the tropical Pacific, in SEAsia, Philippines and Indonesia there is a strong preference for LO in EN conditions and HI in LN. In Indonesia this tendency is year-round, while in SEAsia and the Philippines rates for LO in EN are strongest in the second quarter of the year while those for HI in LN are strongest in the first quarter.

In NEAustralia there are moderate rates for LO in EN throughout the second half of the year, and a strong HI in LN impact in NDJ preceded by weaker rates in seasons 9–11. Similarly in SEAustralia there are moderate rates, with LO in EN favoured in seasons 8–11, and HI in LN in seasons 9–12.

On the African continent, the Sahel is another region where the relation between rainfall and ENSO has been used in statistical long-range forecasts issued by the Met Office since the 1980s (Folland et al., 1991), along with other SST-related predictors. The analysis of rates of occurrence shows a weakly significant tendency for LO in EN and HI in LN in the mid-year rainy season, and an opposite tendency for HI in EN in seasons 10 and 11 when rainfall is seasonally very low. The EAfrica region climatology features a double rainfall season, with 'long rains' in the second quarter and 'short rains' in the fourth quarter of the year. No clear ENSO impact is evident in the rates for the 'long rains', but moderate rates for HI in EN appear during the 'short rains'. In SSAfrica the main impact is in DJF with strong rates for LO in LN and moderate rates for HI in LN, and similar weaker rates in surrounding seasons.

Within Europe, impacts are evident in SWEurope where weak to moderate rates for HI in EN and LO in LN appear in seasons 8–11, and some evidence for a reversed effect in MAM. Again there is an associated reversal of N34 versus PR seasonal correlations.

There are several examples of two or more consecutive seasons with 0/9 rates of occurrence in the regional analysis of GPCP 1979–2012. The most extensive is in the Philippines, with rates of 0 for HI in EN in seasons 11,12,1–5 and also for LO in LN for seasons 8–12,1–5. Others are: Indonesia for HI in EN in seasons 7,8 and 11,12,1, and LO in LN in seasons 11,12,1–3; SSAfrica for LO in LN in seasons 1–3; NSAmerica for HI in EN in seasons 1,2; SSAmerica for HI in LN in seasons 11,12,1; MexUSA for LO in EN in seasons 10–12,1; SEUSA for both LO in EN and HI in LN in seasons 1,2; Caribbean for LO in EN in seasons 2,3, and for LO in LN in seasons 8–10; SEAsia for HI in EN in seasons 3–6 and 10,11; and SEAustralia for both HI in EN and LO in LN in seasons 10,11.

Overall the DJF and JAS tendencies in Table 6 qualitatively agree with the information in the regression maps for those seasons in Yang and DelSole (2012), Figs. 6 and 7. As was the case for T impacts, regions with substantial regression signals do not necessarily have significant rate of occurrence values. For example, in EChina there are substantial negative regression values in JAS, but the rates of occurrence slightly favour the opposite signal.

In some regions the very large EN events in 1982–83 and 1997–98 have impacts contrary to the most common effect. For example, among the regions and seasons listed in Table 5, in NEUSA MAM and WSAmerica JFM the outcome was HI PR rather than LO PR during these strong EN events.

Discussion

The use of contingency tables calculated from categorised historical data is a straightforward way of analysing ENSO impacts, and provides a probabilistic point of view. In investigating the relations between ENSO (with Niño3.4 sea surface temperature N34 as an index) and gridded seasonal precipitation PR and near-surface land temperature T data, three categories were used for each variable. For seasonal precipitation and land temperature the HI (LO) category represented the upper (lower) third of values occurring in the period analysed. For the seasonal N34 index the EN (LN) category represented the upper (lower) quarter of values: with this choice these categories corresponded closely to El Niño and La Niña events. The ratio of, for example, the number of HI and EN entries to the number of EN events for a given location and season is a measure of the rate of occurrence of HI values given EN conditions. Thus the rate of occurrence is an estimate of the odds of a particular outcome in given circumstances, which is more directly relevant for contingency planning and risk management purposes than other common types of ENSO impact statistics such as correlations or composites.

The analysis is subjective in some respects, such as the choices of category boundaries, significant rate levels, detrending, datasets and sample sizes. The objective is to provide a broad overview of the distribution, seasonality and level of impacts,

and we have found that the resulting 'big picture' is not very sensitive to the choices made. We have not attempted here to classify events in more detail, to investigate the effects of ENSO type ('central Pacific' vs 'east Pacific') or magnitude, or the influence of major volcanic eruptions. For some regions these factors may make a qualitative difference: for example, in Fig. 8 the contrasting effect on temperature in northwest Europe of very large El Niño events is evident. For regional applications that may have special considerations (such as risks associated with particular thresholds of climatic variables), a more focussed analysis is recommended for specific purposes.

We have described the results in several ways. The maps (Figs. 3, 4, 10, and others in the Supplementary material) contain the geographical distribution of rates of occurrence, highlighting locations where the rates are unlikely to have such high (or low) values by chance. (We have used the term 'significant' for rates that have roughly a 5–10% chance of arising at random, based on contingency table statistics.) The four panels in each figure show the rates for HI and LO outcomes given EN conditions, and for HI and LO in LN conditions. Note that the geographic detail in the results is limited by the horizontal resolution of the gridded datasets employed. A wide (but not exhaustive) selection of area averages is used to illustrate the main regional impacts. In Table 2 (temperature) and Table 5 (precipitation) comparative values of rates for two data sources are provided for select seasons. In most cases results from the two sources are quite similar. Rates vary considerably with season, and in Tables 3 and 6 the seasonal variations are summarised for each region. Qualitatively the main features described in the text agree with ENSO impacts identified in various ways in previous analyses.

In several regions the effect of ENSO reverses during the seasonal cycle: e.g. EN may have a HI impact in part of the year and a LO impact in another (e.g. for temperature in NEAustralia, Table 3), or EN and LN may both have a HI impact in different seasons (e.g. for temperature in NENAmerica, Table 3). This type of behaviour is usually associated with a change in sign of the seasonal correlation between the Niño3.4 index and the regional T or PR timeseries. However, a change in correlation sign does not necessarily mean significant rate levels are attained for opposite impacts.

Information from our analyses of rates of occurrence was used to prepare schematic maps to summarise the locations and seasonality of the main impacts. In deciding the content, we bore in mind that rates are not precise, and that the 'significance' levels used in the descriptions in preceding sections are somewhat arbitrary: the use of seasonal cycle information was useful in looking for seasonal spells with similar effects in various sectors. Examples are provided in Figs. 12 and 13, which indicate land temperature and precipitation effects favoured during El Niño. Further schematic maps for La Niña conditions are provided in Section D of the Supplementary material. These maps are subjective, and not geographically or seasonally precise, but rather are intended to provide a concise overview. Impacts will vary within the areas highlighted, and impacts may occur beyond those areas. Certainly the details of ENSO impacts are more complicated than can be conveyed in these simplified views.

It is important to bear in mind that while the statistics of historical data provide guidance regarding the extent, seasonality and level of typical impacts, each ENSO event is individual, and occurs alongside other climatic events in ever-varying combinations. Thus maps like those in this article for typical effects should not be regarded as a prediction of the consequences of a particular current event, in progress or foreseen. For that purpose more relevant information is contained in

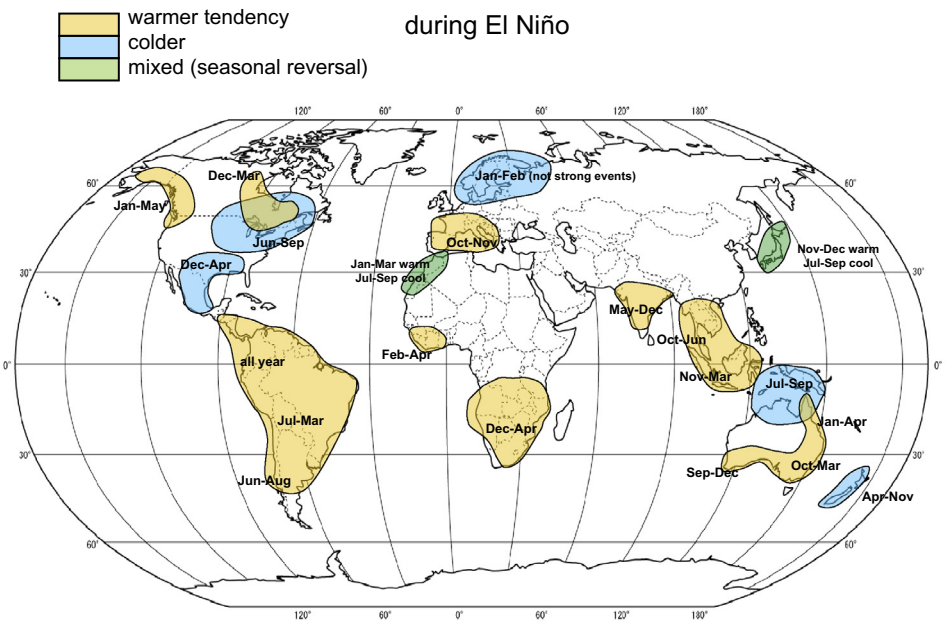

Fig. 12. A schematic map indicating the location and seasonality of the typical land temperature effects that are favoured during El Niño events, according to the rate of occurrence analyses.

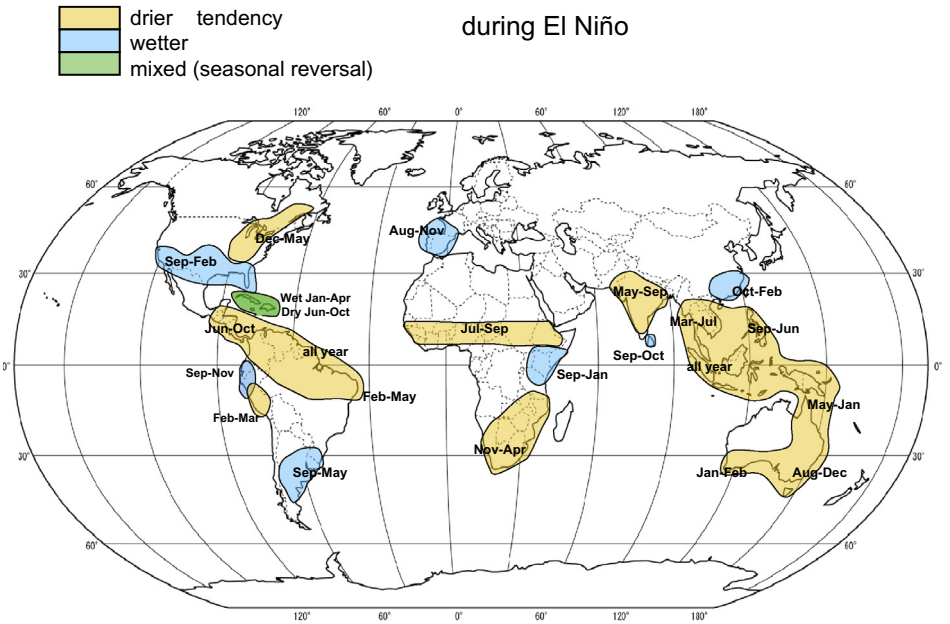

Fig. 13. A schematic map indicating the location and seasonality of the typical precipitation effects in land regions that are favoured during El Niño events, according to the rate of occurrence analyses.

Table 7
A list of acronyms and abbreviations.

ENSO	El Niño Southern Oscillation
SOI	Southern Oscillation Index
EN	El Niño
LN	La Niña
T	(Near surface) temperature
PR	Precipitation
HI	High (T or PR) i.e. in the top third of values
LO	Low (T or PR) i.e. in the bottom third of values
ENHI	El Niño and high (T or PR)
N34	Niño3.4, a region in the equatorial Pacific
LRF	Long-range forecast
NCEP	National Centers for Environmental Prediction
CMAP	Climate Prediction Center Merged Analysis of Precipitation
GPCP	Global Precipitation Climatology Project
CRUTEM	Climate Research Unit Temperature
HadISST	Hadley Centre Ice and Sea Surface Temperature
SST	Sea surface temperature
JFM	January, February, March

Likewise ENLO = El Niño and low, LNHI = La Niña and high, LNLO = La Niña and low.
Likewise FMA denotes February, March, April, and so on for other three-month seasons.
Season 1 is December, January, February; season 2 is January, February, March, etc.

the real-time regional long-range forecasts produced by various prediction centres that take into account recent observational data and prevailing global and local conditions.

To close, we note that the rate of occurrence statistics described here may also be employed in the comparative assessment of climate model performance. The rates for several regions are thus being calculated routinely for Met Office climate models and compared with observed values to contribute to a wide-ranging evaluation process.

Acknowledgements

The work undertaken for this article was supported by the joint DECC/Defra Met Office Hadley Centre Climate Programme (GA01101). The HadISST version and CRUTEM version 4.1.1.0 data were obtained from http://www.metoffice.gov.uk/hadobs/. The NCEP and CMAP and GPCP version 2.2 data were obtained from http://www.esrl.noaa.gov/psd/data/gridded/.

Appendix A. Supplementary data

Supplementary data associated with this article can be found, in the online version, at http://dx.doi.org/10.1016/j.crm.2013.12.002.

References

Adler, R.F., Huffman, G.J., Chang, A., Ferraro, R., Xie, P., Janowiak, J., Rudolf, B., Schneider, U., Curtis, S., Bolvin, D., Gruber, A., Susskind, J., Arkin, P., Nelkin, E., 2003. The version 2 Global Precipitation Climatology Project (GPCP) monthly precipitation analysis (1979–present). J. Hydrometeor. 4, 1147–1167.

Bell, C.J., Gray, L.J., Charlton-Perez, A.J., Joshi, M.M., Scaife, A.A., 2009. Stratospheric communication of El Niño teleconnections to European winter. J. Climate 22, 4083–4096.

Brönnimann, S., 2007. Impact of El Niño-Southern Oscillation on European climate. Rev. Geophys. 45. http://dx.doi.org/10.1029/2006RG000199.

Brönnimann, S., Xoplaki, E., Casty, C., Pauling, A., Luterbacher, J., 2007. ENSO influence on Europe during the last centuries. Climate Dyn. 28, 181–197.

Couper-Johnston, R., 2000. El Niño – The Weather Phenomenon that Changed the World. Hodder & Stoughton.

Dee, D.P., Uppala, S.M., Simmons, A.J., Berrisford, P., Poli, P., Kobayashi, S., Andrae, U., Balmaseda, M.A., Balsamo, G., Bauer, P., Bechtold, P., Beljaars, A.C.M., van de Berg, L., Bidlot, J., Bormann, N., Delsol, C., Dragani, R., Fuentes, M., Geer, A.J., Haimberger, L., Healy, S.B., Hersbach, H., Hólm, E.V., Isaksen, L., Kållberg, P., Köhler, M., Matricardi, M., McNally, A.P., Monge-Sanz, B.M., Morcrette, J.-J., Park, B.-K., Peubey, C., de Rosnay, P., Tavolato, C., Thépaut, J.-N., Vitart, F., 2011. The ERA-Interim reanalysis: configuration and performance of the data assimilation system. Quart. J. R. Meteor. Soc. 137, 553–597.

Folland, C., Colman, A.W., Rowell, D.P., Davey, M.K., 2001. Predictability of Northeast Brazil rainfall and real-rime forecast skill 1987–1998. J. Climate 14, 1937–1958.

Folland, C., Owen, J., Ward, M.N., Colman, A., 1991. Prediction of seasonal rainfall in the Sahel region using empirical and dynamical methods. J. Forecasting 10, 21–56.

Glantz, M.H., 1996. Currents of Change – El Niño's Impact on Climate and Society. Cambridge University Press.

Halpert, M.S., Ropelewski, C.F., 1992. Surface temperature patterns associated with the Southern Oscillation. J. Climate 5, 577–593.

Hoerling, M.P., Kumar, A., Zhong, M., 1997. El Niño, La Niña, and the nonlinearity of their teleconnections. J. Climate 10, 1769–1786.

Jones, P.D., Lister, D.H., Osborn, T.J., Harpham, C., Salmon, M., Morice, C.P., 2012. Hemispheric and large-scale land surface air temperature variations: an extensive revision and an update to 2010. J. Geophys. Res. 117. http://dx.doi.org/10.1029/2011JD017139.

Kalnay, E., Kanamitsu, M., Kistler, R., Collins, W., Deaven, D., Gandin, L., Iredell, M., Saha, S., White, G., Woollen, J., Zhu, Y., Chelliah, M., Ebisuzaki, W., Higgins, W., Janowiak, J., Mo, K.C., Ropelewski, C., Wang, J., Leetmaa, A., Reynolds, R., Jenne, R., Joseph, D., 1996. The NCEP/NCAR 40-year reanalysis project. Bull. Am. Meteor. Soc. 77, 437–470.

Kenyon, J., Hegerl, G.C., 2008. Influence of modes of climate variability on global temperature extremes. J. Climate 21, 3872–3889.

Kenyon, J., Hegerl, G.C., 2010. Influence of modes of climate variability on global precipitation extremes. J. Climate 23, 6248–6262.

Kiladis, G.N., Diaz, H.F., 1989. Global climatic anomalies associated with extremes in the Southern Oscillation. J. Climate 2, 1069–1090.

Mason, S.J., Goddard, L., 2001. Probabilistic precipitation anomalies associated with ENSO. Bull. Am. Meteor. Soc. 82, 619–638.

Morice, C.P., Kennedy, J.J., Rayner, N.A., Jones, P.D., 2012. Quantifying uncertainties in global and regional temperature change using an ensemble of observational estimates: the HadCRUT4 data set. J. Geophys. Res. 117. http://dx.doi.org/10.1029/2011JD017187.

Moron, V., Gouirand, I., 2003. Seasonal modulation of the ENSO relationship with sea level pressure anomalies over the North Atlantic in October–March 1873–1996. Int. J. Climatol. 23, 143–155.

Rayner, N.A., Parker, D.E., Horton, E.B., Folland, C.K., Alexander, L.V., Rowell, D.P., Kent, E.C., Kaplan, A., 2003. Global analysis of sea surface temperature, sea ice, and night marine air temperature since the late nineteenth century. J. Geophys. Res. 108. http://dx.doi.org/10.1029/2002JD002670.

Robock, A., 2000. Volcanic eruptions and climate. Rev. Geophys. 38, 191–219.

Ropelewski, C.F., Halpert, M.S., 1987. Global and regional scale precipitation patterns associated with the El Niño/Southern Oscillation. Mon. Weath. Rev. 115, 1606–1626.

Ropelewski, C.F., Halpert, M.S., 1989. Precipitation patterns associated with the high index phase of the Southern Oscillation. J. Climate 2, 268–284.

Ropelewski, C.F., Halpert, M.S., 1996. Quantifying Southern Oscillation–precipitation relationships. J. Climate 9, 1043–1059.

Someshwar, S., 2009. El Niño Teleconnections in Africa, Latin America and Caribbean, and Asia Pacific. International Research Institute for Climate and Society.

Sterl, A., Van Oldenborgh, G.J., Hazeleger, W., Burgers, G., 2007. On the robustness of ENSO teleconnections. Clim. Dyn. 29, 469–485.

Stone, R.C., Hammer, G.L., Marcussen, T., 1996. Prediction of global rainfall probabilities using phases of the Southern Oscillation index. Nature 384, 252–255.

Toniazzo, T., Scaife, A.A., 2006. The influence of ENSO on winter North Atlantic climate. Geophys. Res. Lett. 33. http://dx.doi.org/10.1029/2006GL 027881.

Trenberth, K.E., Branstator, G.W., Karoly, D., Kumar, A., Lau, N.-C., Ropelewski, C., 1998. Progress during TOGA in understanding and modelling global teleconnections associated with tropical sea surface temperatures. J. Geophys. Res. 103 (C7), 14291–14324.

Troccoli, A., Harrison, M., Anderson, D.L.T., Mason, S.J. (Eds), 2008. Seasonal Climate: Forecasting and Managing Risk, NATO Science Series, vol. 82.

Van Oldenborgh, G.J., Burgers, G., 2005. Searching for decadal variations in ENSO precipitation teleconnections. Geophys. Res. Lett. 32. http://dx.doi.org/10.1029/2005GL023110.

Xie, P., Arkin, P., 1997. Global precipitation: a 17-year monthly analysis based on gauge observations, satellite estimates, and numerical model outputs. Bull. Am. Meteorol. Soc. 78, 2539–2558.

Yang, X., DelSole, T., 2012. Systematic comparison of ENSO teleconnection patterns between models and observations. J. Climate 25, 425–446.